"Anatometabolic" Tumor Imaging: Fusion of FDG PET with CT or MRI to Localize Foci of Increased Activity

Richard L. Wahl, Leslie E. Quint, Richard D. Cieslak, Alex M. Aisen, Robert A. Koeppe and Charles R. Meyer

Departments of Radiology and Internal Medicine, Division of Nuclear Medicine, University of Michigan Medical Center, Ann Arbor, Michigan

Positron emission tomographic (PET) images of visceral cancers are commonly visualized as "hot spots" of increased activity with relatively little normal anatomy discernable, when 2-[^{18}F]-fluoro-2-deoxy-D-glucose (FDG) is used as the tracer. We describe a method by which computed tomography or magnetic resonance anatomic images can be digitally fused in three dimensions, using a rigid rotate-translate scale model with PET "metabolic" images, to simultaneously display registered anatomic and metabolic information. Such "anatometabolic" fusion images were produced in 10 patients with a variety of visceral cancers. External fiducial markers placed during both the anatomic and the metabolic study, as well as internal anatomic fiducials defined from landmarks observed on reconstructed transmission images, were used to achieve image fusion. The mean error magnitude ± s.e.m. of fiducial registration in the nine patients with successful realignments was 5.0 ± 0.8 mm. The mean accuracy in realignment between known anatomic structures seen on both the anatomic study and on the emission PET scan (but not used in realignment) was 6.3 ± 0.8 mm. Localization of foci of increased FDG uptake to specific anatomic structures was achieved by this method, which represented an enhancement over the rudimentary anatomy available from the emission images alone. Anatometabolic fusion images made using this reasonably simple method should prove useful in the management of patients with cancer and other diseases.

J Nucl Med 1993; 34:1190–1197

A positron-emitting analog of glucose, 2-[^{18}F]-fluoro-2-deoxy-D-glucose (FDG), rapidly accumulates in many human neoplasms following intravenous injection (*1–11*). Indeed, when the FDG accumulation of neoplasms is compared to that of most normal tissues, a relatively high target-to-background ratio is often observed (*7,8*).

Although high target-to-background ratios are useful for tumor detection, they may also be problematic if tumor uptake of FDG is so high that relatively little soft-tissue background activity is identified. In such cases, determining where foci of increased FDG uptake are located can be difficult. This problem is even more apparent with high contrast parametric images (*12*). Fusion of metabolic emission images from positron emission tomography (PET) to the much higher resolution anatomic information available from magnetic resonance imaging (MRI) or computed tomography (CT) scans seems desirable (*13*). This approach has been applied by several groups to fuse PET or single-photon emission computed tomography (SPECT) emission images of the brain with MR or CT anatomic images (*14,19*). Indeed, tracer uptake has been mapped onto patient-specific or atlas-based brain anatomy (*14–23*). Since the normal brain has reasonably high levels of FDG uptake throughout it and moderate anatomic information is available, anatomic information from emission brain images can be used in the realignments (*18,24*).

Whereas anatomically defining the location of PET tracer uptake in the brain is feasible, the situation in the body, where many normal tissues have much lower levels of FDG accumulation than the brain and thus provide less anatomy, is more challenging. In addition, while the brain and its contents are fixed, the body can twist and bend. In the present study, we demonstrate the feasibility of digital image fusion between body PET and MRI or CT to produce hybrid "anatometabolic" images of the body, which contain both the exquisite anatomic detail of CT or MRI and the unique physiological information from PET. This is achieved using a rigid rotate-translate scale model and a realignment algorithm based on operator-identification of external markers present on both emission PET and CT/MRI as well as, in some instances, unique anatomic points defined on both transmission PET images and the anatomic study.

METHODS

Ten patients were studied. Each patient was >18 yr old and provided written informed consent for participation in the study. The PET studies were performed as parts of ongoing clinical

Received Oct. 19, 1992; revision accepted Feb. 16, 1993.
For correspondence or reprints contact: Richard L. Wahl, MD, Division of Nuclear Medicine, University of Michigan Medical Center, 1500 E. Medical Center Drive, B1G412, Ann Arbor, MI 48109-0028.

TABLE 1
Accuracy of Fusion in Ten Patients with Anatometabolic Tumor Imaging

Pt. no.	Cancer	Modality	Number of fiducials (e,i)*	Mean error magnitude (mm)	Mean accuracy of realignment† (mm)
1	Breast	MR	4 (1,3)	4.6	6.2 (3)
2	Testis	MR	8 (8,0)	4.0	8.4 (3)
3	Testis	MR	8 (8,0)	5.6	9.3 (4)
4	Prostate	MR	5 (3,2)	5.5	7.3 (3)
5	Bladder	MR	5 (5,0)	5.1	4.4 (2)
6	Lung	CT	4 (3,1)	2.3	6.6 (4)
7‡	Bladder	MR	5 (5,0)	10.4‡	24.8‡ (1)
8	Lung	CT	5 (4,1)	3.6	1.0 (2)
9	Lung	CT	5 (1,4)	11.0	7.4 (3)
10	Lung	CT	4 (1,3)	3.7	6.1 (3)
Mean ± s.e.m.				5.04 ± 0.82	6.3 ± 0.81

*e = number of external fiducials; i = number of internal fiducials used in realignment.
†Number in parentheses is number of points assessed for accuracy of fusion.
‡Technically unsatisfactory due to patient motion during emission PET study and was not used in calculating mean error magnitude or accuracy.

protocols to evaluate the diagnostic accuracy of PET in a variety of cancers. The study population is briefly described in Table 1.

PET images were acquired with a Siemens CTI 931/08-12 PET scanner (Siemens Medical, Iselin, NJ). The method for image acquisition has previously been described and 15 slices of ~6.8-mm thickness were obtained per scanning level (*8, 10, 11*). In brief, transmission PET datasets were first obtained over specific areas of the body suspected of containing cancer for a period of ~10 min per set of 15 slices (with axial coverage of ~10 cm) using the retractable $^{68}Ge/^{68}Ga$ ring transmission sources of the PET scanner. Transmission images were reconstructed by filtered backprojection and generally contained 5–10 million detected coincidence events per image. Following the performance of one or more transmission scans, radioactive fiducial markers were taped onto ink-marked skin sites on the patient that were expected to be within the field of view of the scanner. These fiducial markers contained 0.5–3 μCi of FDG adsorbed onto ~2–5-mm diameter polystyrene beads. Markers were placed so that the suspected tumor region was thoroughly surrounded by markers (generally covering 15–20 cm in the z-axis). Up to eight markers were placed per patient. Emission images reconstructed using filtered back-projection were obtained following the intravenous injection of approximately 10 mCi of FDG. The two 10-min duration images from 50–70 min postinjection were used for fusions. Generally ~20 cm of the patient was imaged in the z-axis, which represented two contiguous 10-cm acquisitions. A 128 × 128 image matrix display was used to display emission images of approximately 8 mm resolution.

Six patients had MR scans obtained with a Picker Vista 0.5 Tesla or GE Signa 1.5 Tesla MRI device. Standard T1-weighted, T2-weighted and/or proton density spin-echo images were obtained, which were 5–10 mm in slice thickness, generally with a 1-mm gap between images. Images were displayed using a 256 × 256 image matrix. Vitamin E capsules (100 I.U. vitamin E, Rorer Inc., Ft. Washington, PA) were taped over the same marked skin sites used for the PET imaging study and were oriented perpendicular to the axial scan plane. Anisotropic markers were chosen because of their improved visibility, their commercial availability and their ability to define the geometric center of the markers.

CT scans were obtained in four patients in the standard fashion with or without intravenous contrast, depending on the clinical situation. A GE 9800 CT (General Electric Medical Systems, Milwaukee, WI) scanner was used with a 2-sec scan time. Images were displayed using a 512 × 512 pixel image matrix. Small cylindrical lead markers, roughly 2 mm in diameter × 1.0 cm in length, were placed over the same marked skin sites used for the PET study, oriented perpendicular to the scan plane. Generally, 1-cm thick contiguous tomographic sections slices were obtained. In some cases the anatomic study preceded the PET scan. In each case, however, the PET and anatomic studies were performed on the same day. During each imaging procedure, efforts were made to position the patient straight and flat on their backs on the scanning table but no external frames were used.

Image Fusion

All cross-sectional image sets were reconstructed initially on each acquisition system using standard vendor-supplied reconstruction algorithms. Image fusions were performed on a Sun 4 workstation running Sun OS Unix and the native MIT X-windows graphical user interface. Reconstructed datasets were transferred to the workstation using the Internet file transfer protocol. To reduce the spatial granularity of z-axis identification of marker location, all image sets were first interpolated in the z-axis direction using a fourth-order, Hamming-weighted sinc function to yield three evenly separated interpolated images for every original cross-sectional image. The sinc function was chosen because of its particular suitability for reconstructing sample data sets (*25*). The z-axis interpolation maintained anisotropic voxels, i.e., "cuberiles" were not made. Note that the interpolated dataset was used only for determining geometric transformation. Identification of corresponding three-dimensional markers (homologous point pairs) in each dataset were selected by the operator using mouse-driven, paired slider-scrolled images and pointer. The center of the fiducial markers was used in the realignments. After point pairs were identified in the datasets, a rigid rotate-scale-

translate geometric model for dataset realignment was derived from the usual unconstrained least mean square error affine solution, C_{lmse} (*26*). If $C_{lmse} = U S V'$, where the columns of U are the eigenvectors of C_{lmse} corresponding to the eigenvalues on the diagonal matrix S and where U, S and V are obtained from the singular value decomposition of C_{lmse}, then the rotation matrix estimate is obtained from U V' (transpose of V), and the scaling matrix is estimated from the diagonal of U S U', where U' is the transpose of U. Additional constraints on the scaling matrix included limiting x-, y- and z-axis scaling to calibration (1.00) plus or minus 20%. With this transformation algorithm, the geometrically transformed PET voxels are thus computed using trilinear interpolation and then displayed upon the reference CT or MRI voxels. In this way, only the PET data were re-sampled. This was done to: (a) maximally preserve the anatomic data from the higher resolution CT or MR studies and (b) because the trilinear interpolation is best performed on lower frequency data sets (i.e., PET).

Initial attempts at image fusion were performed using only external fiducial markers visible on both the anatomic and emission PET studies. These provided satisfactory first approximation fusions, although two problems were apparent. First, on some occasions, some markers were not included in the field of view of both scans. This could result from the exclusion of some markers seen on CT or MRI from the PET images due to the limited z-axis field of view of the PET scanner. Second, it was recognized that changes in the shape of skin surface anatomy did not always accurately reflect changes in deep anatomy. This problem was most apparent in the thoracic scans, as patients studied by CT for standard diagnosis were examined while at suspended, full inspiration with the arms up, as compared to free-breathing with the arms down for the more lengthy PET examination. For example, markers placed near the shoulders for PET could move out of the field of view on CT and thus were not usable for realignment.

For this reason, the reconstructed transmission PET images were also used to define internal anatomic points that could be directly digitally transferred onto the emission PET images (as transmission and emission PET images were perfectly registered, if there was no patient motion) and then identified on CT/MR. In the thorax, unique locations in three-space that were easily seen on most transmission image sets included the carina and the lung apices. In the abdomen, less internal anatomy was apparent, but in the pelvis, the center of a radiopaque prosthetic femoral head was seen clearly on transmission images in one patient. Thus, both external fiducials and internal markers seen on transmission scan (and digitally transferred to the emission scan) were used in the fusion algorithms (Table 1). The anatomic points defined on the PET transmission images were in the first several patients defined by a radiologist (RLW), but were subsequently identified by a trained technologist. The external fiducials were readily defined by a technologist.

The accuracy of the fusions was assessed both qualitatively (visual analysis for obvious misalignment) and quantitatively using two types of measurements: One measurement was a computer-generated estimate of the mean error vector magnitude between the marker points selected on the CT/MR anatomic images and the resulting position of markers on the emission PET images after fusion was complete. The second measurement was of the accuracy of independently locating anatomic structures seen on the emission PET images (but not used in realignments) and the same structures on the anatomic images after registration. Examples of such structures include (in the thorax) the top of the aortic arch, center of the aorta, and in the abdomen, the upper or lower poles of the kidneys, or the center of blood vessel, etc. Since multiple areas of the body were imaged, the same anatomic sites could not be used in all cases. Mean accuracy of realignment was thus defined between the emission PET and the relevant anatomic study for 1–4 points/patient (Table 1). A flow chart describing the overall method of realignment is shown in Figure 1.

RESULTS

The characteristics of the patients studied, anatomic imaging modality fused with PET, fiducial characteristics and the quantitative accuracy of the fusion imaging are presented in Table 1. By qualitative visual assessment, successful fusion of anatomic and metabolic images was achieved in nine of the ten patients. In one patient (No. 7), patient motion occurred during the emission PET imaging study, resulting in a poor quality PET study and substantial uncertainty in defining the location of the radioactive fiducial markers. Quantitative analysis supported the visual impression of suboptimal realignment. In the nine patients (Patient 7 is excluded) with qualitatively acceptable fusions, the mean error magnitude across fiducial markers following image fusion was 5.04 ± 0.82 mm. The accuracy of realignment, determined by comparing point-by-point locations of known structures visualized on both the anatomic and metabolic studies, but not used to produce the realignments, was 6.3 ± 0.81 mm.

In six of the patients, and all of the patients in whom the thorax was imaged, a combination of the external fiducial markers and internal-fiducial points placed on the emission PET images by direct data transfer following examination of the reconstructed transmission images were used in the realignment process. The most consistently identified internal fiducial point on transmission images was the carina, although the lung apices could also be readily located if included in the field of view. In one patient, a pulmonary nodule was visible on both CT and transmission PET, with its center providing a point for realignment (Patient 9). In this thoracic patient, realignment was worse than in any other qualitatively satisfactory patient. This was almost certainly due to the difference in thoracic configuration between the two studies, caused by the different physiological states present during their acquisition (i.e., CT was at near full inspiration, while emission and transmission PET images represented an average of tidal breathing, with a resultant lower lung volume).

The display format for the fusion images is shown in Figure 2 for a patient with a history of treated metastatic germ cell carcinoma of the testes, who was studied by both MRI and FDG PET. The fusion image demonstrates fidelity of realignment of the markers and of the cardiac ^{18}F activity with the myocardium seen on MRI and of the dome of the liver with modest hepatic ^{18}F activity. The area of concern for tumor on MRI, a retrocardiac nodule, was seen as a "cold" area on PET and on follow-up months later was unchanged. This is most compatible with

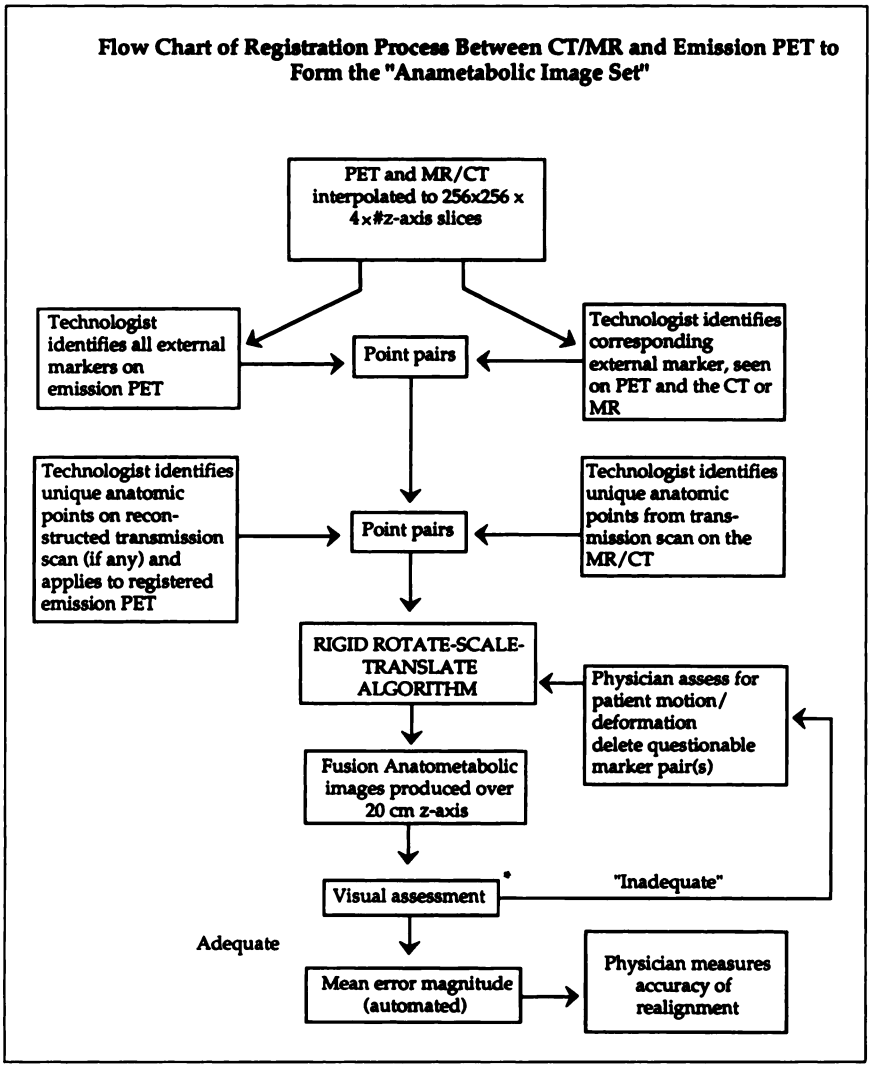

FIGURE 1. Flow chart detailing method of anatometabolic image formation (after Ref. 18).

a representation of stable scarring after aggressive chemotherapy (*7,27*).

The potential of the method in the care of a patient with newly diagnosed lung cancer is illustrated in Figure 3A. In this patient, CT shows volume loss in the right lower lung and a localized right pleural effusion. The corresponding PET image shows intense central FDG uptake with a small focus of modest FDG uptake in the anterior left chest, with only minimal FDG uptake elsewhere. The fusion image clearly demonstrates intense FDG uptake in the central portion of the right lower lobe collapse. This appearance is most consistent with central FDG-avid lung cancer, whereas the peripheral area represents postobstructive lung volume loss with little FDG uptake. A lower set of images (Fig. 3B) shows that the anterior left chest FDG activity is myocardial in origin. This fusion over multiple image planes illustrates that the fusions are true fusions in three dimensions, not just realignments within a single imaging plane.

The ability of our algorithm to realign volumes of tissue is also clearly shown in a patient with metastatic breast cancer (Fig. 4). Images high in the thorax (Fig. 4A), in the mid-thorax (Fig. 4B) and in the mediastinum (Fig. 4C) show excellent alignment. Three foci of increased FDG uptake were difficult to localize on emission PET alone due to the high target-to-background ratios. The fusion image demonstrated that there was focal tumor in an anterior right rib and not in a lymph node as was suspected without the fusion images (Fig. 4B). An unexpected observation was two foci of intense FDG uptake in the mediastinum (Fig. 4C). The fusion image (Fig. 4C) showed that the FDG uptake was into normal-sized lymph nodes. On follow-up studies several months later, this patient had progressive systemic and mediastinal involvement with breast cancer, which implied that PET detected cancer in normal-sized lymph nodes. Such cases where FDG activity localizes to apparently normal structures on anatomic imaging studies would seem to represent a situation in which anatometabolic fusion imaging would be of great value.

Fusion imaging was also possible in the abdomen, although external fiducial markers were more necessary than in the chest because relatively little internal anatomic information was provided by transmission images of the abdomen. In our small series, there were no quantitative

differences in the quality of realignments in comparing the chest and abdomen (Table 1). For example, in a patient being evaluated as a part of an ongoing study of prostatic carcinoma, excellent image realignment was achieved (Fig. 5). This individual had an abnormal bone scan and T1-weighted MR image with metastatic prostatic carcinoma to the acetabulum/hip region. Emission PET demonstrated two foci of FDG activity, one of moderate intensity in the prostate itself (he had residual prostatic carcinoma in the gland), and a more intense triangular focus to the right of the prostate. Fusion images showed the right-most activity to be in the right acetabulum (Fig. 5, bottom).

Although realignments with our current algorithm are sometimes imperfect (such as in Patient 7) and more sophisticated warping algorithms might be useful, it is clear that our relatively simple approach, which can align to within 5–6 mm, has practical utility.

DISCUSSION

Our study demonstrates that it is possible to obtain reasonably accurate anatometabolic fusion images between CT or MR and FDG/PET scans by using a relatively simple rotate-translate-scale rigid model and manual identification of fiducial points from the CT, MR and transmission and emission PET images. These anatometabolic images appear to be particularly useful in defining the anatomic location of intense foci of FDG uptake that are otherwise difficult to localize precisely due to limited background activity.

The method we describe, using both external fiducial markers and available internal points of anatomy (derived from transmission images), is a unique approach to realignment. The use of the transmission data in addition to the

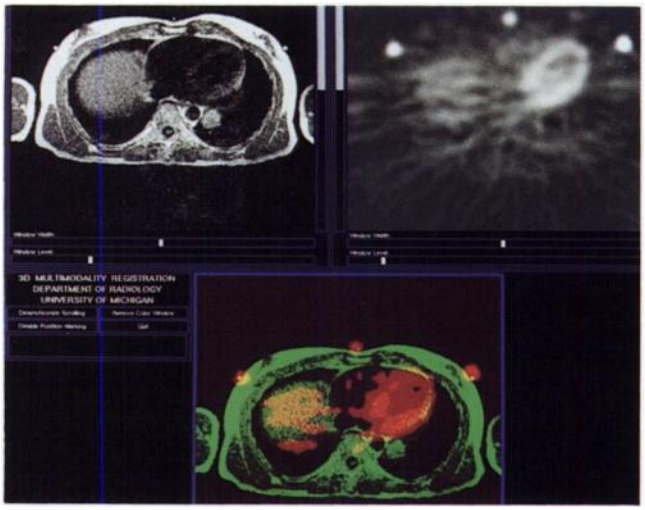

FIGURE 2. Patient with a history of germ cell carcinoma of the testis with multiple stable residual pulmonary nodules following aggressive chemotherapy. The upper left hand image is a T1-weighted (TR 667, TE 20) spin-echo MR image showing a retrocardiac nodule, a small nodule at the right costo-phrenic angle and three vitamin E markers positioned over the anterior chest. The FDG PET emission image at 60 min postinjection (upper right) clearly shows the three FDG fiducial markers at the same skin locations as the vitamin E markers, myocardial FDG uptake and a small photopenic area in the retrocardiac area. The fusion image (bottom) shows excellent registration between the FDG and vitamin E markers, demonstrates FDG uptake in the cardiac wall and shows no FDG uptake in either pulmonary nodule. Modest FDG uptake projects in the expected location for the liver. Follow-up of this patient showed stability of the pulmonary nodules most consistent with scarring and a lack of FDG accumulation.

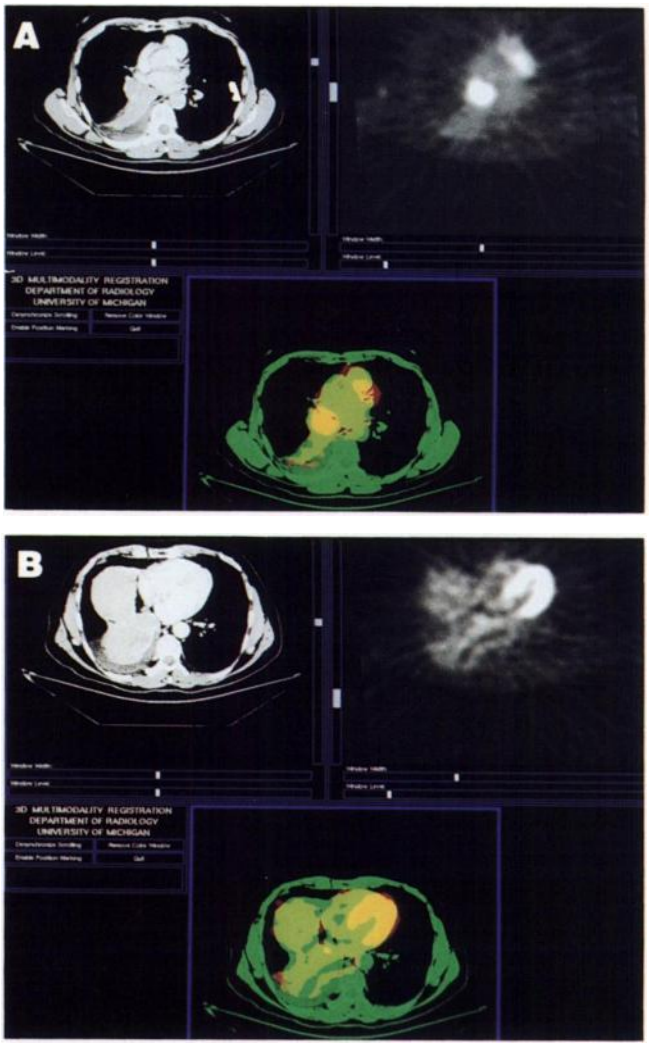

FIGURE 3. (A) CT shows marked volume loss in the right lower lung and a localized right pleural effusion in a patient with newly diagnosed lung cancer. The corresponding transverse emission PET image obtained at 60 min postinjection shows intense central FDG uptake in the right chest, modest focal FDG uptake in the anterior left chest, but only minimal FDG uptake in the blood pool and the collapsed right lower lobe/effusion area. The fusion image (bottom) clearly demonstrates intense FDG uptake in the central portion of the collapsed right lower lung most consistent with uptake in the central tumor, whereas the remainder of the right lung has activity most consistent with postobstructive volume loss. MRI performed elsewhere supported this interpretation and the large central tumor was treated nonsurgically. (B) A more caudal series of images from the same patient as in (A) demonstrates that the left anterior chest activity seen in (A) is myocardial in origin, with the left ventricular wall clearly delineated by PET, despite its poor delineation on the CT study. This is best seen on the fusion image.

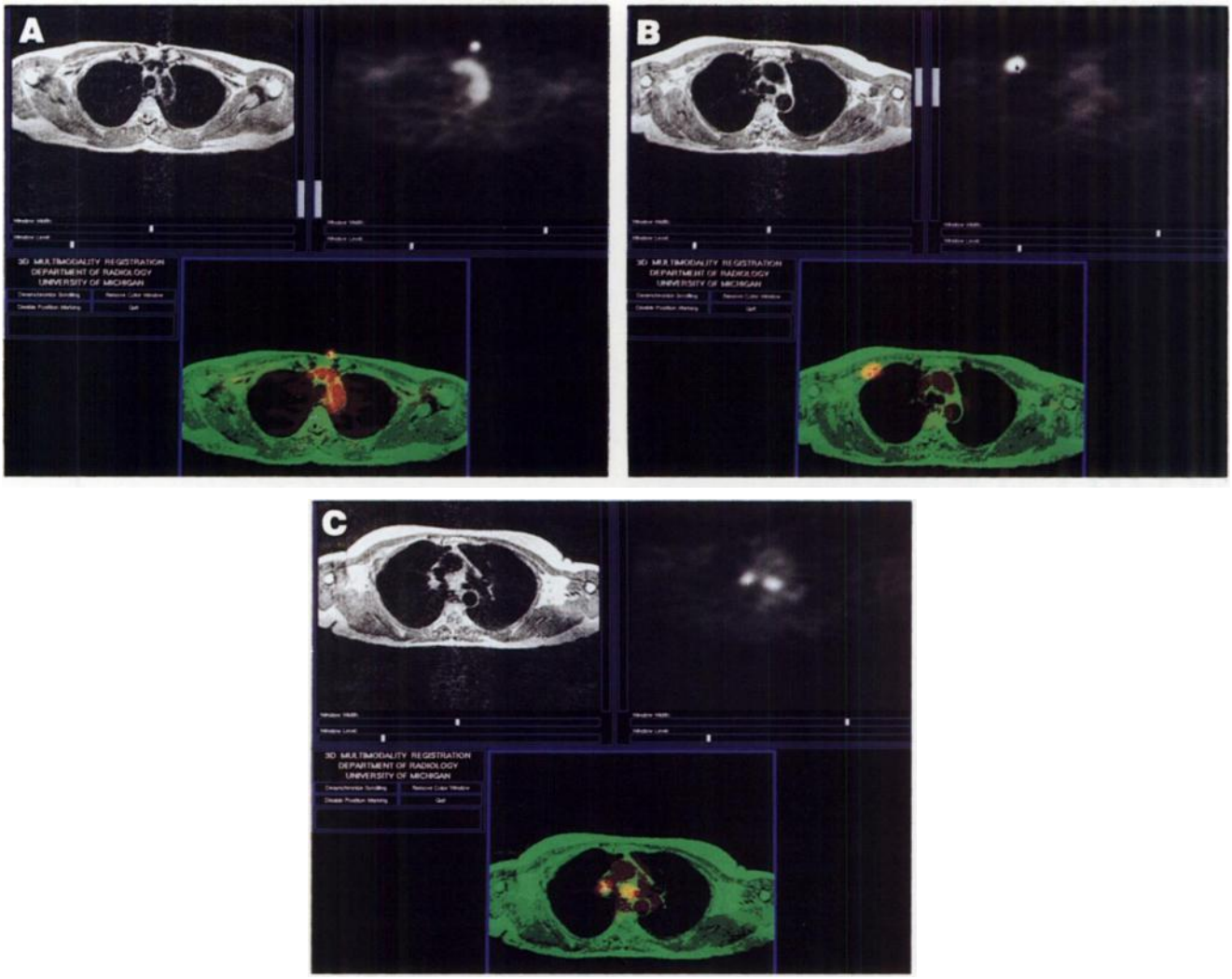

FIGURE 4. (A) Images of the upper chest in a woman with metastatic breast cancer show a marker over the upper sternum on both proton-density (TR 2600, TE 30) MR (upper left) and emission PET (upper right). PET shows residual FDG activity in the blood vessels (windowed to allow vessel visualization at 60 min postinjection). Fusion image (bottom) shows excellent registration between the FDG marker on emission PET and the vitamin E marker on MRI. Direct superimposition of the blood-pool FDG activity onto MRI-defined upper thoracic blood vessels is seen. (B) At a somewhat lower level, an intense focus of FDG uptake is noted in the right anterior chest region. This focus is difficult to localize on emission PET alone, due to its high target-to-background ratio, and could represent either chest wall or a possible axillary lymph node focus of increased FDG activity. Proton-density MRI demonstrates focal expansion and distortion of an anterior right rib. The fusion image superimposes intense FDG uptake into this abnormal rib, which is consistent with an FDG-avid rib metastasis. (C) Two foci of intense FDG uptake were also seen in the mediastinum of this patient on emission PET (upper right). Proton-density MRI of this area was interpreted as essentially normal (upper left). The fusion image placed the increased FDG uptake into borderline normal-sized lymph nodes (lower image). Eight months postscanning, the patient had CT, which demonstrated progressive breast cancer in multiple locations, including the mediastinum. Thus, clinical follow-up strongly suggests that FDG uptake was in borderline normal-sized, but tumor-involved, lymph nodes.

external markers helps deal with problems that can arise due to differences in anatomic shape between internal structures of the body and external structures. For instance, in our experience, the fiducial point for localization of the carina from the reconstructed transmission images is very useful in performing PET/CT realignment in the chest. Defining the carina simply by extrapolation of the relationship of external markers between MRI and PET or CT and PET is more difficult because of the change in thoracic configuration between the two studies.

Pitfalls with our technique include:

1. The possibility that the patient has "twisted" between MR/CT and PET imaging.
2. Changes in the patient's bowel gas content or urine content could change anatomy in the upper or lower abdomen.
3. Respiratory or other motion may make realignment difficult.
4. The patient could move during the PET (or MR/CT) study.

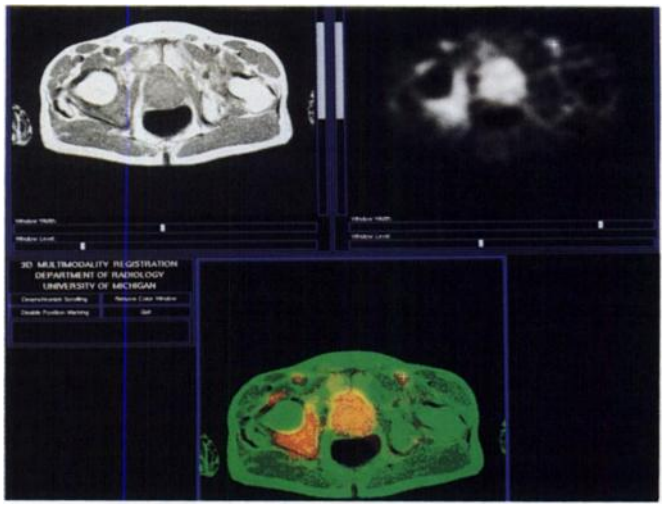

FIGURE 5. T1-weighted MRI (TR 600, TE 20) demonstrates abnormal signal intensity in the region of the right acetabulum in this patient with metastatic prostatic carcinoma to bone. Emission PET demonstrated two foci of FDG activity, one in the midline and one to the right of midline. Fusion images demonstrated that the focal uptake in the midline was in the region of the prostate gland (the patient had residual prostate carcinoma in the gland), and the signal from the right of midline fused into the area of abnormal MR signal (metastasis) located in the right acetabulum. Fidelity of the fusion was further substantiated by the fact that the two faint foci of FDG uptake located anterior and to either side of the prostate were seen at multiple levels on PET (i.e., were tubular) and fused into the location of the external iliac blood vessels.

5. Surface anatomy (and thus marker location) is variant between the two studies, such as in very obese patients where a change in the appearance of the pannus of fat (and markers on it) might not reflect internal anatomy.

These issues are partly addressed since we have been careful to perform the anatomic and physiologic studies on the same day with the patient laid carefully onto his/her back, in a similar state of hydration or feeding. Obviously, more sophisticated algorithms which include the ability to "warp" the three-dimensional image datasets between the two studies would be ideal for more precise realignment.

Our approach to realignment and registration of body PET studies with CT or MRI is related to several of the approaches described for fusing brain PET or SPECT images with MR or CT images (*14–22,24*). The realignment algorithms for brain anatomic and emission studies have taken several forms, but the situation in the brain is simpler than in the body because the brain and skull do not substantially deform between studies. For the brain, realignment algorithms have been described that eliminate the need for surface markers. One such algorithm uses the transmission-scan defined surface of the skull and the surface of the scalp on MRI or CT to perform realignments (*14,15,17*). This so-called "head in the hat" algorithm searches for minima in the quality of surface realignments, but is not totally operator-independent. This approach reportedly requires ~2–3 hr/patient to complete (*17*).

Another approach to realigning MR and PET images of the brain does not require external markers or transmission images. This involves defining the interhemispheric plane on both MR and emission PET, with subsequent operator interactions to produce realignments in the other dimensions (*18*). Although this approach is said to require less than an hour of processing, it can require user definition of points on the emission PET scan, including the border between the "gray matter and CSF." This can be difficult due to the poor resolution of PET versus CT or MRI and because white matter mainly adjoins the CSF. This algorithm is also reported to be less successful if the interhemispheric fissure is nonplanar (*18*).

The preceding approaches for brain image registration reported "error magnitudes" in the 3–4 mm range. Our error magnitude of 5–6 mm compares well with these, particularly considering that the body is much more subject to deformation than the brain. There is, however, some uncertainty in our assessment of accuracy of realignment as it is sometimes challenging to accurately define the location of vessels on emission PET, and with some vessels, to uniquely define their z-axis location is not possible.

While it may become feasible in the future to eliminate the need for skin surface markers in the realignment algorithm, a trained technologist can prepare and apply markers in a few minutes. In most cases, one technologist applied the ^{18}F markers and another applied the vitamin E or lead markers, so a "devoted" technologist was not essential. Careful attention to positioning the patient "flat" on the imaging table was employed.

A trained technologist was able to perform the computer realignment procedure in less than 2 hr, often without assistance from a radiologist. This seems an advantage over methods requiring a greater familiarity with emission PET and MRI anatomy than the modest knowledge of anatomy needed to define points on the transmission images with our method (*18*). In our realignment algorithm, anatomic input from a physician is to assess the subjective quality and quantitative accuracy of realignment and to determine if patient motion occurred.

A rapid reliable fusion method for body imaging that does not require external fiducials would be preferable to our method. By incorporating anatomic data from the transmission images, we moved in this direction and were able to achieve successful fusions using as few as one external fiducial marker in three of our patients. Clearly, the method we applied is less cumbersome than having the patient rigidly immobilized in a mold or frame, as has been done in brain imaging studies (*22,29*). It should be noted that fusion images and/or extraction of region of interest information also have shown promise in better localizing abnormalities seen on SPECT imaging using ^{99m}Tc-red blood cells for hemangioma detection and with SPECT of radiolabeled monoclonal antibodies (*30–32*). This suggests a more general applicability of such fusion methods.

In summary, we describe a method which allows for the fusion of CT or MR anatomic images in three dimensions

with PET metabolic images to produce a series of anatometabolic images. The method involves the use of external fiducial markers for all imaging modalities and is further refined through the use of internal landmarks from foci in the body that are uniquely defined on both the transmission PET images and the CT or MRI study. Such anatometabolic information should prove useful in anatometabolic directed biopsies of areas most likely to contain active cancer that may appear normal by other imaging tests (*29*).

While additional experience and simplification will be necessary to routinely apply our method to clinical practice, we believe that our relatively simple approach will prove practical in those clinical situations in which reasonably exact anatomic delineation of the origin of the ^{18}F (or other PET tracer) signal is necessary. Indeed, as techniques to produce image fusions become simpler, such anatometabolic images may well become the standard for PET image display in patients with cancer and other illnesses.

ACKNOWLEDGMENTS

The authors thank the technologists and chemists of the University of Michigan PET Center for their assistance and Ms. Manette London, Annette Betley, Barbara Burton, and Joan Fogarty for their contributions. Supported by NIH grants 5 RO1 CA53172, 1 R55 CA52880, CA and MO1 RR00042, as well as the "Hi-tech funding initiative" from the University of Michigan Hospital.

REFERENCES

1. Som P, Atkins HL, Bandoypadhyay D, et al. A fluorinated glucose analog, 2-fluoro-2-deoxy-D glucose (F-18): nontoxic tracer for rapid tumor detection. *J Nucl Med* 1980;21:670–675.
2. Di Chiro G, LeLaPaz RL, Brooks RR, et al. Glucose utilization of cerebral gliomas measured by ^{18}F fluorodeoxyglucose and positron emission tomography. *Neurology* 1982;32:1323–1329.
3. Yonekura Y, Benua RS, Brill AB, et al. Increased accumulation of 2-deoxy-2-[^{18}F]fluoro-D-glucose in liver metastases from colon carcinoma. *J Nucl Med* 1982;23:1133–1137.
4. Paul R, Ahonen A, Roeda D, Nordman E. Imaging of hepatoma with 18F-fluorodeoxyglucose [Letter]. *Lancet* 1985;1:50–51.
5. Strauss LG, Clorius JH, Schlag P, et al. Recurrence of colorectal tumors: EPT evaluation. *Radiology* 1989;170:329–332.
6. Minn H, Soini I. Fluorine-18 fluorodeoxyglucose scintigraphy in diagnosis and follow up of treatment in advanced breast cancer. *Eur J Nucl Med* 1989;15:61–66.
7. Wahl RL, Hutchins GD, Buchsbaum DJ, Liebert M, Grossman HB, Fisher S. Fluorine-18-2-deoxy-2-fluoro-D-glucose (FDG) uptake into human tumor xenografts: feasibility studies for cancer imaging with PET. *Cancer* 1991; 67:1544–1550.
8. Wahl RL, Cody RL, Hutchins GD, Mudgett EE. Primary and metastatic breast carcinoma: initial clinical evaluation with PET with the radiolabeled glucose analogue 2-[F-18]-fluoro-2-deoxy-D-glucose. *Radiology* 1991;179: 765–770.
9. Griffeth LK, Dehdashti F, McGuire AH, McGuire DJ, Perry DJ, Moerlein SM. PET evaluation of soft-tissue masses with fluorine-18 fluoro-2-deoxy-D-glucose. *Radiology* 1992;182:185–194.
10. Wahl RL, Harney J, Hutchins G, Grossman HB. Imaging of renal cancer using FDG PET: pilot animal and human studies. *J Urol* 1991;146:1470–1474.
11. Harney JV, Wahl RL, Liebert M, et al. Uptake of 2-deoxy, 2-(18F)fluoro-d-glucose in bladder cancer: animal localization and initial patient positron emission tomography. *J Urol* 1991;145:279–283.
12. Wahl RL, Zasadny KR, Greenough R, Koeppe R. Parametric image displays to enhance visualization of cancers using FDG/PET: influx constant and temporal subtraction imaging [Abstract]. *Radiology* 1991;181:152.
13. Wahl RL, Meyer C, Koeppe R, Aisen A, Quint LE. Where is the tumor imaged on FDG PET scanning as a "hot spot"? Methods for metabolic/anatomic registration [Abstract]. *Radiology* 1991;181:151.
14. Levin DN, Pelizzari CA, Chen GTY, Chen C-T, Cooper MD. Retrospective geometric correlation of MR, CT, and PET images. *Radiology* 1988;169: 817–823.
15. Pelizzari CA, Chen GTY, Spelbring DR, Weichselbaum RR, Chen C-T. Accurate three-dimensional registration of CT, PET and/or MR images of the brain. *J Comp Assist Tomogr* 1989;13:20–26.
16. Alpert NM, Bradshaw JF, Kennedy D, Correia JA. The principal axes transformation—a method for image registration. *J Nucl Med* 1990;31:1717–1722.
17. Holman BL, Zimmerman RE, Johnson KA, et al. Computer-assisted superimposition of magnetic resonance and high-resolution technetium-99m-HMPAO and thallium-201 SPECT images of the brain. *J Nucl Med* 1991; 32:1478–1484.
18. Kapouleas I, Alavi A, Alves WM, Gur RE, Weiss DW. Registration of three-dimensional MR and PET images of the human brain without markers. *Radiology* 1991;181:731–739.
19. Fox PT, Perlmutter JS, Raichle ME. A stereotactic method of anatomical localization for positron emission tomography. *J Comp Assist Tomogr* 1985; 9:141–153.
20. Bohm C, Greitz T, Kingsley D, Berggren BM, Olsson L. Adjustable computerized stereotaxic brain atlas for transmission and emission tomography. *Am J Neuroradiol* 1983;4:731–733.
21. Mazziotta JC, Pelizzari CC, Chen GT, Bookstein FL, Valentino D. Region of interest issues: the relationship between structure and function in the brain. *J Cereb Blood Flow Metab* 1991;11(suppl 1):A51–A56.
22. Evans AC, Beil C, Marrett S, Thompson CJ, Hakim A. Anatomical-functional correlation using an adjustable MRI-based region of interest atlas with positron emission tomography. *J Cereb Blood Flow Metab* 1988;8:513–530.
23. Vannier MW, Gayou DE. Automated registration of multimodality images. *Radiology* 1988;169:860–861.
24. Friston KJ, Passingham RE, Nutt JG, Heather JD, Sawle GV, Frackowiak RSJ. Localization of PET images: Direct fitting of the intercommissural (AC-PC) line. *J Cereb Blood Flow Metab* 1989;9:690–695.
25. Papoulis A. *The Fourier integral and its applications.* New York: McGraw Hill; 1962:52.
26. Noble B, Daniel JW. *Applied linear algebra.* Englewood Cliffs, NJ: Prentice Hall; 1988:346–350.
27. Wahl RL, Harney JV, Hutchins GD, Grossman HB. PET imaging of GU neoplasms: initial evaluation. Presented at 76th Scientific Assembly and Annual Meeting, RSNA, 1990.
28. Bookstein FL. Principle warps: thin plate splines and the decomposition of deformation. *IEEE Trans Pattern Anal Med Intell* 1989;11:567–585.
29. Zhang J, Levesque MF, Wilson CL, et al. Multimodality imaging of brain structures for stereotactic surgery. *Radiology* 1990;175:435–441.
30. Birnbaum BA, Noz ME, Chapnick, et al. Hepatic hemangiomas: Diagnosis with fusion MR, CT, and Tc-99m-labeled red blood cell SPECT images. *Radiology* 1991;181:469–474.
31. Kramer EL, Noz ME, Sanger JJ, Megibow AJ, Maguire GQ. CT-SPECT fusion to correlate radiolabeled monoclonal antibody uptake with abdominal CT findings. *Radiology* 1989;172:861–865.
32. Kramer EL, Noz ME. CT-SPECT fusion for analysis of radiolabeled antibodies: applications in gastrointestinal and lung carcinoma. *Int J Rad Appl Instrum [B]* 1991;18:27–42.